Tsunami generation by dynamic displacement of sea bed due to dip-slip faulting

Denys Dutykh, Frédéric Dias

To cite this version:

Tsunami generation by dynamic displacement of sea bed due to dip-slip faulting

Denys Dutykh, Frédéric Dias

CMLA, ENS Cachan, CNRS, PRES UniverSud, 61 Av. President Wilson, F-94230 Cachan, France

Abstract

In classical tsunami-generation techniques, one neglects the dynamic sea bed displacement resulting from fracturing of a seismic fault. The present study takes into account these dynamic effects. Earth's crust is assumed to be a Kelvin-Voigt material. The seismic source is assumed to be a dislocation in a viscoelastic medium. The fluid motion is described by the classical nonlinear shallow water equations (NSWE) with time-dependent bathymetry. The viscoelastodynamic equations are solved by a finite-element method and the NSWE by a finite-volume scheme. A comparison between static and dynamic tsunami-generation approaches is performed. The results of the numerical computations show differences between the two approaches and the dynamic effects could explain the complicated shapes of tsunami wave trains.

1 Introduction

The accuracy of the computation of the whole life of a tsunami, from generation to inundation, obviously depends on the construction of the initial condition. This is why the process of tsunami generation must be modelled as accurately as possible. Even though the constraint of being able to predict tsunami arrival time, height and location as fast as possible must be taken into account (in other words, a trade-off must be found between the precision and the speed of computation of the initial condition), we believe that so far the scientific community has not payed enough attention to the crucial subject of tsunami generation.

After the pioneering work of Kajiura [10] it has become a common practice in the tsunami community to translate the static sea bed deformation generated by an underwater earthquake onto the free surface and let it propagate. We will refer to this method as *passive approach*. The validity of this technique was already discussed in [16,3]. Three-dimensional (3D) analytical expressions derived from Volterra's formula applied to the general study of dislocations [13,17] are used to construct the

static initial deformation. Similar analytical expressions for two-dimensional (2D) problems were also derived by Freund & Barnett [4], who used the theory of analytic functions of a complex variable. The popularity of these analytic solutions can be explained by their relatively simple explicit form. Thus, their computation is easy and inexpensive. A feature of the solution of Freund & Barnett is that nonuniform slip distributions can be considered. In particular, slip distributions which remove the singular behavior of the internal stresses at the ends of the slip zone can be dealt with, simply by imposing the so-called smooth closure condition on the slip: the slip is zero at the ends.

When simplifying hypotheses such as homogeneity or isotropy are removed, analytical solutions are no longer available and the governing equations must be solved numerically. Static deformations caused by slip along a fault have been extensively simulated by Masterlark [14], who used several dislocation models based on the finite-element method (FEM) to estimate the importance of different physical hypotheses. Anisotropy and heterogeneity turned out to be the most important factors in this type of modelling. Megna et al. [15] also used the FEM to compare numerical results with analytical solutions. However neither in [14] nor in [15] were the dynamical aspects and the coupling with hydrodynamics considered. Moreover the consequences for the resulting tsunami waves were not pointed out.

When one uses as initial condition a static seismic source together with the translation of the sea bed deformation onto the free surface, one neglects the rupture velocity and the rise time. Several studies have already been performed to understand wave formation due to different prescribed bottom motions by introducing either some type of rise time or some type of rupture velocity. For example, Todorovska & Trifunac [24] studied the generation of waves by a slowly spreading uplift of the bottom. Hammack [7] generated waves experimentally by raising or lowering a box at one end of a channel, and considered various laws for the rise or the fall of the box. In their review paper, Dutykh & Dias [2] generated waves theoretically by multiplying the static deformations caused by slip along a fault by various time laws: instantaneous, exponential, trigonometric and linear. Haskell [8] was one of the first to take into account the rupture velocity. In fact he considered both rise time, T, and rupture velocity, V. Consider the source shown in Figure 1. The two horizontal coordinates x and y, and the vertical coordinate z are denoted by $\vec{x} = (x, y, z)$. Let
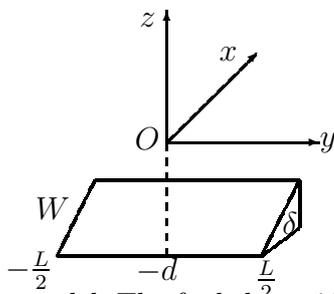

Fig. 1. Geometry of the source model. The fault has width W, length L, depth d and dip angle δ.

2

$\vec{b}(\vec{x}, t)$ denote the fault displacement function and $\vec{b}_0(\vec{x})$ the final displacement. The following form for $\vec{b}(\vec{x}, t)$ was considered by Haskell:

$$
\vec{b}(\vec{x}, t) = \begin{cases} 0 & t - \zeta/V < 0 \\ (\vec{b}_0/T)(t - \zeta/V) & 0 < t - \zeta/V < T \\ \vec{b}_0 & t - \zeta/V > T \end{cases} \tag{1}
$$

The coordinate ζ is a coordinate along the fault. Eq. (1) implies that at $t = 0$ a fracture front is established instantaneously over a width W of the $y-$axis at depth d. The front propagates unilaterally at constant velocity V over a length $L\cos\delta$ of the $x-$axis. At any fixed point on the fault plane the relative displacement increases at constant velocity from 0 at $t = \zeta/V$ to a constant final value $\vec{b}_0$ at $t = T + \zeta/V$. Okumura & Kawata [19] used Haskell's approach to investigate the effects of rise time and rupture velocity on tsunami generation. They considered two cases of sea bottom motion: (i) with only rise time and (ii) with both rise time and rupture velocity. They found that the effects of rupture velocity are much smaller than those of rise time when the rise time is assumed to be long (over 10 min). Ohmachi et al. [16] also considered rise time and rupture velocity but unfortunately the dynamics is not clearly explained in their paper. Apparently they did not solve the elastodynamic equations with the second-order time derivative (see next section). Another attempt to understand dynamical effects is that of Madariaga [12], who considers a dip-slip dislocation propagating in a half-space and solves the elastodynamic equations by using the double Laplace transform. The solution is elegant but rather complex. Unfortunately no plots of the deformation of the free surface are provided and the coupling with the water layer is not considered either. The present study can be considered as an attempt to understand the coupling between seismic faulting and hydrodynamics by integrating numerically the time-dependent elasticity equations as well as the time-dependent fluid equations. The authors have already adressed the problem of tsunami generation in [3,2]. The main feature of the present study is the use of a more realistic earthquake source model.

The paper is organised as follows. In Section 2 we briefly describe the mathematical models, both for solid and fluid motions. Section 3 contains details on the numerical methods used to solve the governing equations. The numerical method for the solid motion is validated in Section 4. Section 5 provides a comparison between the traditional approach to tsunami generation (in which the static sea bed deformation is translated onto the free surface) and the more realistic approach of dynamic generation (in which the wavetrain is generated by the motion of the bottom). We reveal numerically that the dynamic generation of tsunamis can for example create a leading depression wave when one expects a leading elevation wave.

3

2 Mathematical models

Even though the numerical results shown in this paper are for 2D configurations, the modeling is performed for 3D problems. The horizontal coordinates are denoted by x and y, while the vertical coordinate is denoted by z. The displacements are denoted by u_x, u_y and u_z. We use different origins along the vertical axis for the solid and fluid motions. In the earth domain, $z = 0$ denotes the sea bed at rest (assumed to be flat) while in the fluid domain, $z = 0$ denotes the sea surface at rest.

2.1 Dynamic fault model

The fault is assumed to be inside a geological viscous medium. Earth's crust is assumed to be a viscoelastic material of density ρ. We choose the Kelvin-Voigt viscosity model [20] which consists in using complex elastic coefficients (with negative imaginary parts in order to dissipate wave energy). For isotropic media it means that the Lamé coefficients have a nonpositive imaginary part: $\lambda^* = \lambda_r - i\lambda_i, \quad \mu^* = \mu_r - i\mu_i$, where $\lambda_r, \mu_r > 0$ and $\lambda_i, \mu_i \geq 0$. The classical elasticity equations are obtained by choosing $\lambda_i \equiv 0$ and $\mu_i \equiv 0$. On the time-scales relevant to our problem, elasticity is sufficient and the assumption of a Kelvin-Voigt viscous material is unnecessary. But we keep it for the sake of completeness.

Let c_P and c_S be the classical velocities for the propagation of P and S waves in a medium of density ρ:

$$c_P = \sqrt{\frac{\lambda_r + 2\mu_r}{\rho}}, \quad c_S = \sqrt{\frac{\mu_r}{\rho}}.$$

Complex Lamé coefficients yield complex velocities for wave propagation,

$$c_P^* = c_P\sqrt{1 + i/Q_P}, \quad c_S^* = c_S\sqrt{1 + i/Q_S},$$

where the coefficients Q_P and Q_S are defined as follows:

$$Q_P = -\frac{\lambda_r + 2\mu_r}{\lambda_i + 2\mu_i}, \quad Q_S = -\frac{\mu_r}{\mu_i}.$$

The factors Q_P and Q_S measure the viscosity of the geological medium. In this study we restrict our attention to the weakly viscous case ($1/|Q_P| \ll 1$ and $1/|Q_S| \ll 1$).

Let $\underline{\underline{\sigma}}$ represent the stress tensor. The displacement field $\vec{u}(x, y, z, t) = (u_x, u_y, u_z)$ satisfies the classical elastodynamic equations from continuum mechanics:

$$\nabla \cdot \underline{\underline{\sigma}} = \rho\frac{\partial^2 \vec{u}}{\partial t^2}. \tag{2}$$

It is common in seismology to assume that the stress tensor $\underline{\underline{\sigma}}$ is determined by Hooke's law through the strain tensor $\underline{\underline{\varepsilon}} = \frac{1}{2}\left(\nabla\vec{u} + \nabla^t\vec{u}\right)$. Therefore

$$\underline{\underline{\sigma}} = \lambda^*(\nabla \cdot \vec{u})\underline{\underline{I}} + 2\mu^*\underline{\underline{\varepsilon}}. \tag{3}$$

Thus, we come to the following linear viscoelastodynamic problem [1]:

$$\nabla \cdot \left(\lambda^*(\nabla \cdot \vec{u})\underline{\underline{I}} + \mu^*(\nabla\vec{u} + \nabla^t\vec{u})\right) = \rho\frac{\partial^2\vec{u}}{\partial t^2}. \tag{4}$$

Recall that the mechanical characteristics ρ, λ^* and μ^* can possibly depend on the spatial coordinates (x, y, z). However we will assume that they are constant in the numerical applications.

The fault is modeled as a dislocation inside a viscoelastic material. This type of model is widely used for the interpretation of seismic motion. A dislocation is considered as a surface (in 3D problems) or a line (in 2D problems) in a continuous medium where the displacement field is discontinuous. The displacement vector is increased by the amount of the Burgers vector $\vec{b}$ along any contour C enclosing the dislocation surface (or line), i.e.

$$\oint_C d\vec{u} = \vec{b}. \tag{5}$$

We let a dislocation run at speed V along a fault inclined at an angle δ with respect to the horizontal. Rupture starts at position $x = 0$ and $z = -d$ (it is supposed to be infinitely long in the transverse $y-$direction) and propagates with constant rupture speed V for a finite time L/V in the direction δ stopping at a distance L. Let ζ be a coordinate along the dislocation line. On the fault located in the interval $0 < \zeta < L$ slip is assumed to be constant. The rise time is assumed to be 0.

2.2 Fluid layer model

Since the main purpose is to model tsunami generation processes and since tsunamis are long waves, it is natural to choose the nonlinear shallow water equations (NSWE) as hydrodynamic model. These equations are widely used in tsunami modelling, especially in codes for operational use [25,21]. The validity of the NSWE model and the question of the importance of dispersive effects have already been addressed by the authors in [11].

---

[1] We use the prefix "visco-" due to the presence of the imaginary part in the Lamé coefficients, which is responsible for small wave damping.

Let η denote the free-surface elevation with respect to the still water level $z = 0$, $\vec{v} = (v_x, v_y)$ the horizontal velocity vector, g the acceleration due to gravity and $z = -h(x, y, t)$ the bathymetry. The NSWE in dimensional form read

$$\frac{\partial \eta}{\partial t} + \nabla \cdot ((h + \eta)\vec{v}) = -\frac{\partial h}{\partial t}, \qquad \frac{\partial \vec{v}}{\partial t} + \frac{1}{2}\nabla |\vec{v}|^2 + g\nabla\eta = 0. \qquad (6)$$

The effect of the moving bottom appears in the source term $-\partial h / \partial t$ in the first equation. The unknowns η and $\vec{v}$ are functions of time and of the horizontal coordinates x and y. Since the NSWE are essentially obtained from depth-averaging the Euler equations, the dependence on the vertical coordinate z disappears from the equations. The coupling between the earth and fluid models is made through the function $h(x, y, t)$ which describes the moving sea bottom bathymetry.

3 Numerical methods

In the present study we made two natural choices. The solid mechanics equations are solved using the FEM with fully implicit time integration, while for the hydrodynamic part we take advantage of the hyperbolic structure of the governing equations and use a solver based on the finite-volume scheme (see for example [1,11]).

3.1 Discretization of the viscoelastodynamic equations

In order to apply the FEM one first rewrites the governing equation (4) in variational form. The time-derivative operator is discretized through a classical second-order finite-difference scheme. The method we use is fully implicit and has the advantage of being free of any Courant-Friedrichs-Lewy-type condition. In such problems implicit schemes become advantageous since the velocity of propagation of seismic waves is of the order of 3 to 4 km/s. We apply the $\mathbb{P}2$ finite-element discretization procedure. For the numerical computations, the freely available code FreeFem++ [9] is used.

Let us say a few words about the boundary conditions and the treatment of the dislocation in the program. Concerning the boundary conditions, we assume that the sea bed is a free surface, that is $\underline{\sigma} \cdot \vec{n} = \vec{0}$ at $z = 0$. The other boundaries are assumed to be fixed or, in other words, Dirichlet type boundary conditions $\vec{u} = \vec{0}$ are applied. The authors are aware of the reflective properties of this type of boundary conditions. In order to avoid the reflection of seismic waves along the boundaries during the simulation time, we take a computational domain which is sufficiently large. This approach is not computationally expensive since we use adaptive mesh algorithms [9] and in the regions far away from the fault, element sizes are considerably bigger than in the fault vicinity.

Next we discuss the implementation of the dislocation surface. Across the fault, the displacement field is discontinuous and satisfies the following relation:

$$\vec{u}^+(\vec{x}, t) - \vec{u}^-(\vec{x}, t) = \vec{b}(\vec{x}, t), \tag{7}$$

where the signs $\pm$ denote the upper and lower boundary of the dislocation surface, respectively. The propagation of Burger's vector along the fault is given by

$$\vec{b}(\vec{x}, t) = \vec{b}_0 H(t - \zeta/V), \tag{8}$$

where V is the rupture velocity, H the Heaviside unit step function and ζ a coordinate along the dislocation line.

3.2 Finite-volume scheme for the nonlinear shallow-water equations

Here we briefly describe the discretization of the model (6) by a standard cell-centered finite volume method. The system (6) can be written as

$$\frac{\partial \mathbf{V}}{\partial t} + \nabla \cdot \mathbf{F}(\mathbf{V}) = \mathcal{S}, \tag{9}$$

where $\mathbf{V} = (\eta, u, v)$ is the vector of conservative variables (which coincide here with the physical variables), $\mathcal{S} = (-\partial h/\partial t, 0, 0)$ the source term, and, for every $\mathbf{n} \in \mathbb{R}^2$,

$$\mathbf{F}(\mathbf{V}) \cdot \mathbf{n} = \left((h + \eta)(\vec{v} \cdot \mathbf{n}), \left(\frac{1}{2}|\vec{v}|^2 + g\eta \right) \mathbf{n} \right). \tag{10}$$

The Jacobian matrix $\mathbb{A}(\mathbf{V}) \cdot \mathbf{n}$ is defined by

$$\mathbb{A}(\mathbf{V}) \cdot \mathbf{n} = \frac{\partial (\mathbf{F}(\mathbf{V}) \cdot \mathbf{n})}{\partial \mathbf{V}} = \begin{pmatrix} \vec{v} \cdot \mathbf{n} & (h + \eta)\mathbf{n} \\ g\mathbf{n} & \vec{v} \otimes \mathbf{n} \end{pmatrix}. \tag{11}$$

The computational domain $\Omega \subset \mathbb{R}^2$ is triangulated into a set of control volumes $\Omega = \cup_{K \in \mathcal{T}} K$. We integrate Eq. (9) on K:

$$\frac{d}{dt} \int_K \mathbf{V} \, d\Omega + \sum_{L \in \mathcal{N}(K)} \int_{K \cap L} \mathbf{F}(\mathbf{V}) \cdot \mathbf{n}_{KL} \, d\sigma = \int_K \mathcal{S} \, d\Omega, \tag{12}$$

where $\mathbf{n}_{KL}$ denotes the unit normal vector on $K \cap L$ pointing into L and $\mathcal{N}(K) = \{L \in \mathcal{T} : \operatorname{area}(K \cap L) \neq 0\}$. Then, setting

$$\mathbf{V}_K(t) := \frac{1}{\operatorname{vol}(K)} \int_K \mathbf{V}(\mathbf{x}, t) \, d\Omega \,,$$

we approximate (12) by

$$\frac{d\mathbf{V}_K}{dt} + \sum_{L \in \mathcal{N}(K)} \frac{\operatorname{area}(L \cap K)}{\operatorname{vol}(K)} \Phi(\mathbf{V}_K, \mathbf{V}_L; \mathbf{n}_{KL}) = \mathcal{S}_K \,, \tag{13}$$

where the numerical flux

$$\Phi(\mathbf{V}_K, \mathbf{V}_L; \mathbf{n}_{KL}) \approx \frac{1}{\operatorname{area}(L \cap K)} \int_{K \cap L} \mathbf{F}(\mathbf{V}) \cdot \mathbf{n}_{KL} \, d\sigma$$

is explicitly computed by the FVCF formula of Ghidaglia *et al.* [5]:

$$\Phi(\mathbf{V}, \mathbf{W}; n) = \frac{\mathbf{F}(\mathbf{V}) \cdot \mathbf{n} + \mathbf{F}(\mathbf{W}) \cdot \mathbf{n}}{2} - \operatorname{sgn}(\mathbb{A}_n(\mu(\mathbf{V}, \mathbf{W}))) \frac{\mathbf{F}(\mathbf{W}) \cdot \mathbf{n} - \mathbf{F}(\mathbf{V}) \cdot \mathbf{n}}{2} \,. \tag{14}$$

Here the Jacobian matrix $\mathbb{A}_n(\mu)$ is defined in (11), $\mu(\mathbf{V}, \mathbf{W})$ is an arbitrary mean between $\mathbf{V}$ and $\mathbf{W}$ and $\operatorname{sgn}(M)$ is the matrix whose eigenvectors are those of M but whose eigenvalues are the signs of that of M.

In our problem, the Jacobian matrix (11) has three distinct eigenvalues

$$\lambda_{1,3} = \vec{v} \cdot \mathbf{n} \pm c_s, \quad \lambda_2 = 0,$$

where $c_s = \sqrt{g(h + \eta)}$ is the velocity of long gravity waves. The right and left eigenvectors can be easily computed. Then it is straightforward to compute the sign matrix appearing in (14) and the numerical scheme is thus completely defined.

In this section we did not deal with boundary conditions. This is a complicated topic in finite-volume methods (see [6] for details).

4 Validation of the numerical method

In this section we consider an analytic solution to the line dislocation problem in the static case. Use is made of the well-known result described for example by Freund & Barnett [4] or Okada [17]. In order to simplify the expressions, we only consider the 2D case (in other words, the fault is infinite in the $y-$direction). In fact the best expression is that given by equation (24) in [12]. We checked that it is in full
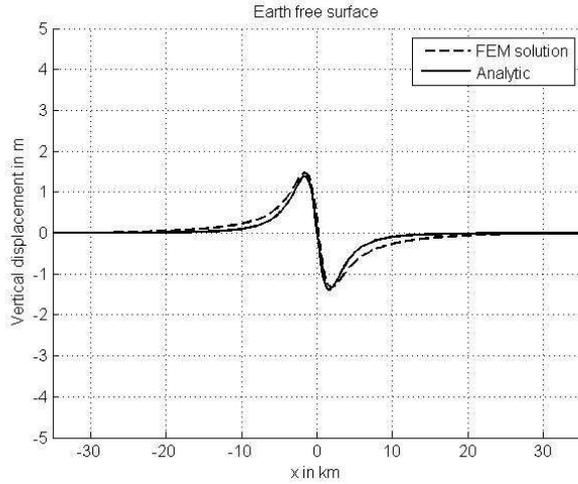
Fig. 2. Comparison between analytical and numerical solutions for a static 2D fault with a dip angle equal to $\pi/2$.

agreement with the limit of Okada's solution as the width becomes infinite. The sketch of the domain is given in Figure 1. The fault has infinite width ($W \to \infty$). Its length is L, its depth d and its dip angle δ.

In the present paper we only give the vertical displacement component u_z along the free surface, since it plays the most important role in tsunami formation. It can be expressed as the difference between two contributions, that from a first dislocation located at the beginning of the fault and that from a second dislocation located at the end of the fault. Let $d_L = d - L \sin \delta$. One has

$$u_z = |\vec{b}_0| \left[U_z \left(\frac{x}{d}, \delta \right) - U_z \left(\frac{x - L \cos \delta}{d_L}, \delta \right) \right], \tag{15}$$

where

$$U_z \left(\frac{x}{d}, \delta \right) = \frac{1}{\pi} \left[\sin \delta \arctan \frac{x}{d} - \frac{d(d \cos \delta - x \sin \delta)}{x^2 + d^2} \right]. \tag{16}$$

For the validation of our numerical method we chose a fault corresponding to a dip angle $\delta = \pi/2$. The values of the other parameters are given in Table 1. This problem was solved by FEM after neglecting the dynamic terms. The results of the comparison with solution (16) are given in Figure 2. Good qualitative and quantitative agreement can be seen. Megna et al. [15], who also considered static displacement due to uniform slip across a normal fault, compared the 2D FEM results with the analytical solution in the case of a normal fault. In their conclusion, they state that it is for the vertical component of the surface displacement that the discrepancies are the largest.
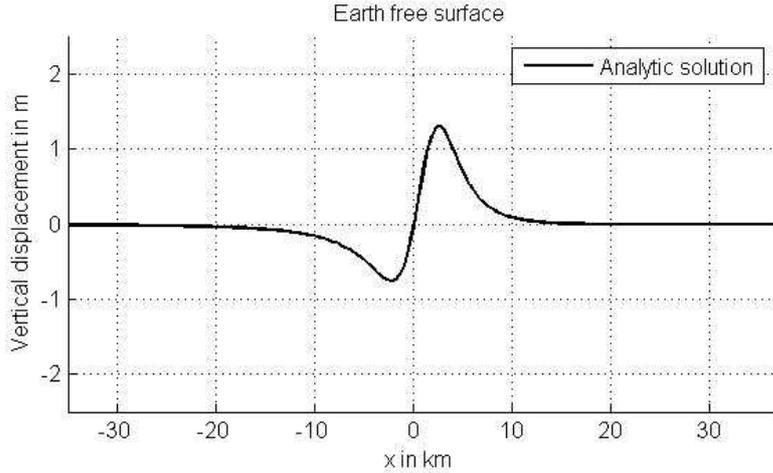
9

Fig. 3. Static deformation due to the dislocation corresponding to the parameters given in Table 1.

Parameter	Value
Young modulus, E, GPa	9.5
Poisson ratio, ν	0.27
Damping coefficient, λ_i	500
Damping coefficient, μ_i	200
Fault depth, d, km	4
Fault length, L, km	2
Dip angle, δ, °	13
Burger's vector length, $|\vec{b}_0|$, m	10
Water depth (uniform), h_0, m	400
Acceleration due to gravity, g, m/s^2	9.8

Table 1
Parameters used in the numerical computations. The water depth and the spatial extent in the main direction of propagation were chosen so that dispersive effects can be neglected.

5   Results of the simulation

In this section, we use the set of physical parameters given in Table 1. The static sea bed deformation obtained with the analytical solution is depicted in Figure 3. Note that the only difference between Figures 2 and 3 is the value of the dip angle.

In order to illustrate the numerical computations we chose several test cases of active/passive tsunami generation. The passive generation approach consists in translating the static sea bed deformation onto the free surface and letting it propagate under gravity [10]. On the other hand, the active approach uses the bottom motion

for wave generation. We proceed by computing the first eight or fifteen seconds of the earthquake dynamics. Then the bottom configuration is assumed to remain frozen during the rest of the simulation. Concerning the dynamical aspects of rupture propagation, we consider the Heaviside-type approach (8) where the dislocation propagates along the fault with rupture velocity V. One could use instead a dislocation for which Burger's vector $\vec{b}_0$ is also space-dependent. But the main goal of the present study is to make an attempt to include the dynamic displacement of the sea bed. In the dynamical approach, we consider three cases: the limiting case where the rupture velocity V is infinite, a fast event with $V = 2.5$ km/s and a slower event with $V = 1$ km/s.

We show below the differences between the passive and the dynamic approaches. This question has already been addressed by the authors [3] in the framework of the linearized potential flow equations and of a simplified model for bottom deformation.

In the first comparison we use a strong coupling between the dynamic displacement of the sea bed and the fluid layer equations and compare it with the passive approach, in which the static solution shown in Figure 3 is translated onto the free surface as initial condition. The rupture velocity V is assumed to be infinite. Moreover the earthquake dynamics is computed during the first eight seconds. The free surface at the beginning of the tsunami generation process is shown on Figure 4. Further steps of this process are given in Figures 5-6. One may have the impression that the passive solution does not evolve. In fact, the explanation lies in the presence of two different time scales in this problem. The fast time scale is provided by the earthquake ($P-$ and $S-$waves) and the slow one by water gravity waves. Since the active generation solution is directly coupled to the bottom dynamics, it evolves with the fast time scale. It is interesting to compare Figures 5 and 6. One can see that the active approach gives at the beginning an amplitude which is almost twice larger but the amplitudes become comparable a few seconds later.

The free-surface elevations are computed until the wave enters the purely propagation stage. This corresponds to Figure 7. One notices that the resulting wave amplitude and velocity are almost the same. Of course the waveform is different. One can see as well that the location of the elevation wave is the same, while the depression wave is slightly shifted. It can be explained by the larger extent of the dynamic solution. Thus, we can conclude from this first comparison that if one is only interested in tsunami travel time or even in rough inundation zone estimation, the passive approach can be used.

The second comparison focusses on the influence of the rupture velocity at two separate times (Figures 8 and 9). The differences between the fast and the relatively slow rupture velocities are small.

The most interesting comparison is the third one, which focusses on the duration of the earthquake. Recall that our somewhat artificial definition of earthquake du-
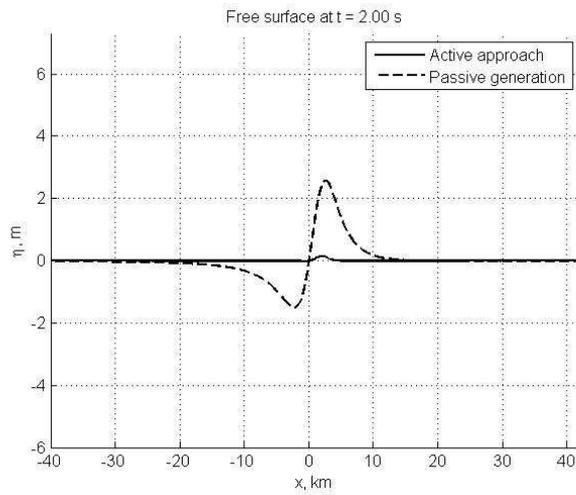
11

Fig. 4. Water free surface at the beginning of the earthquake ($t = 2$s) according to two approaches of tsunami generation: passive versus active (with infinite rupture velocity).
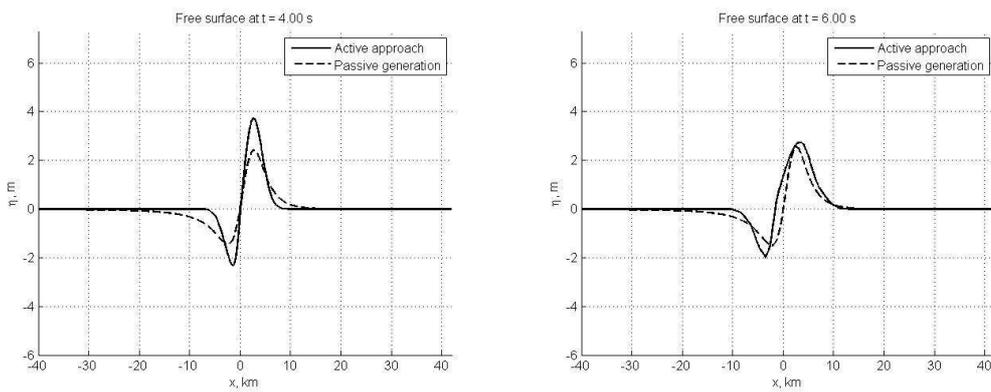
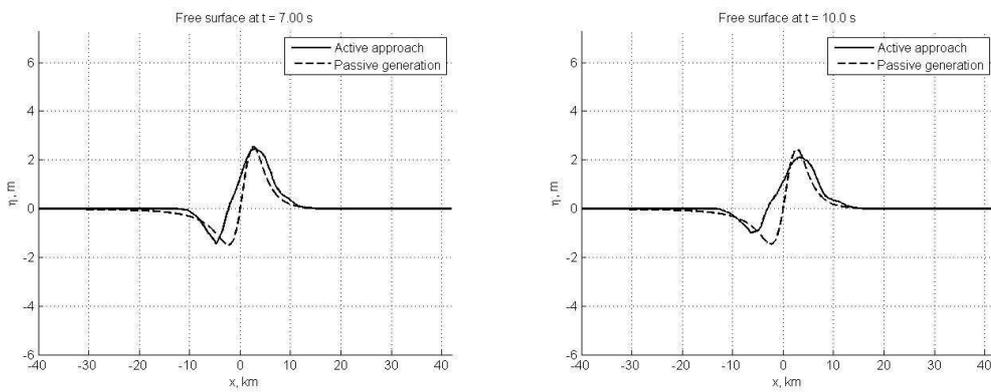

Fig. 5. Same as figure 4 for times $t = 4$s and $t = 6$s.

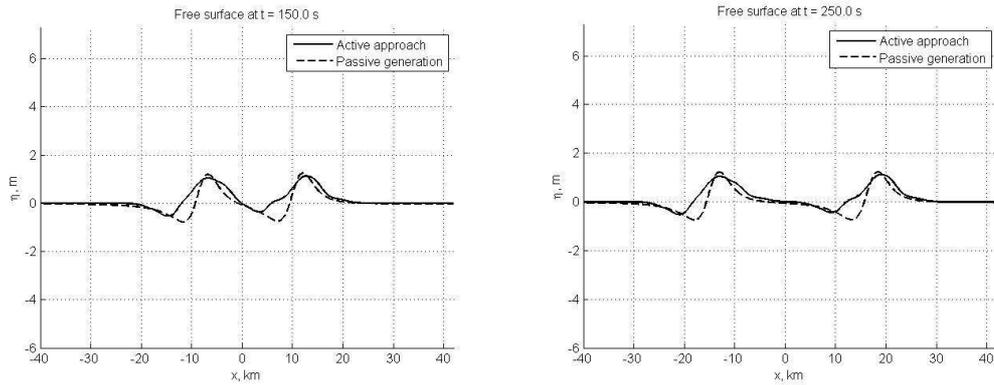
Fig. 6. Same as figure 4 for times $t = 7$s and $t = 10$s.

Fig. 7. Same as figure 4 for times $t = 150$s and $t = 250$s. The wave is leaving the generation zone (left plot) and starting to propagate (right plot).

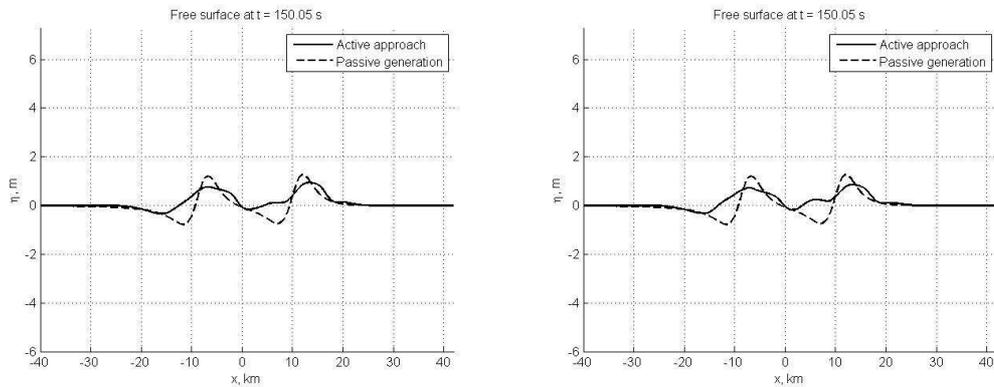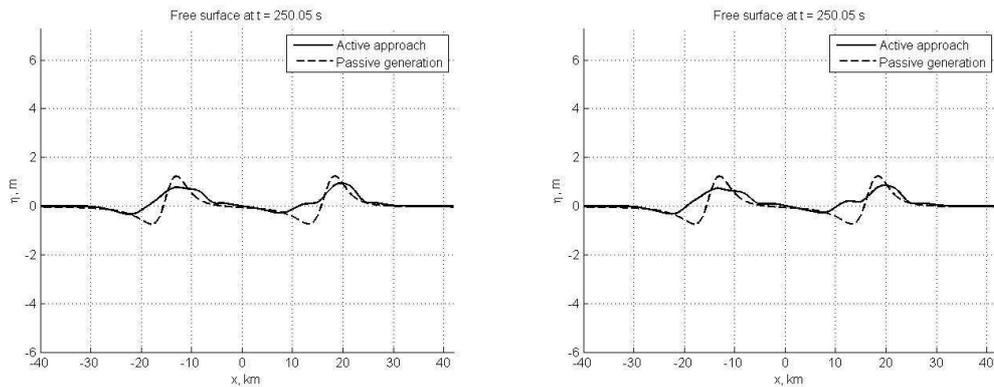Fig. 8. Same as figure 7 (left plot) for two rupture velocities: $V = 1$ km/s (left) and $V = 2.5$ km/s (right).

Fig. 9. Same as figure 8 at time $t = 250$s.

ration is the time at which we stop the bottom motion. After that time, the sea bottom remains frozen. Figure 10 shows the effect of a longer earthquake. One sees that the shapes of the wave train obtained with the dynamic analysis look more complicated than those obtained with the passive analysis. In particular, the distinction between leading elevation wave and leading depression wave is not as clear
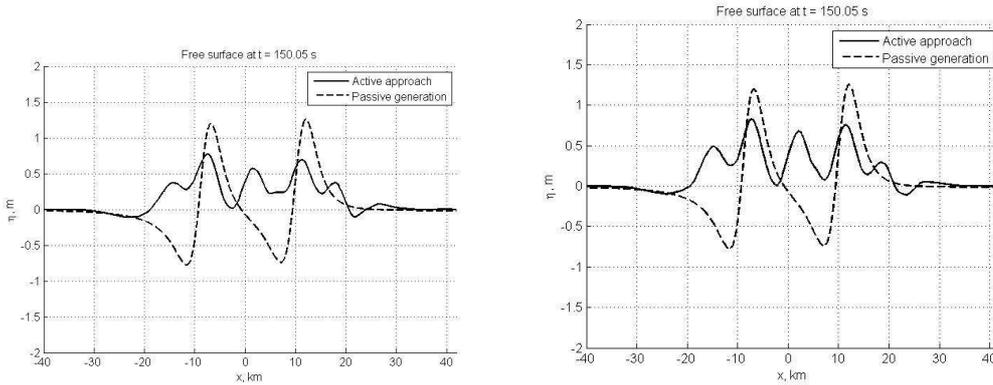
13

Fig. 10. Water free surface at $t = 150$s for a longer earthquake. The motion stops after 15s. The left plot compares the infinite rupture velocity solution with the passive approach. The right plot compares the case of a slow rupture ($V = 1$ km/s) with the passive case.

when using the dynamical analysis. It could be an explanation for the discrepancies between modeled and recorded time series of water levels at various locations along the California coast for the 1960 Chilean tsunami.

6 Conclusions

An approach to model the dynamical character of sea bed deformations during an underwater earthquake was presented. The governing elastodynamic equations were solved by a finite-element method. The principal novelty of the present study is the coupling of the resulting displacement field with the hydrodynamic model.

Two methods for tsunami generation have been compared: static versus dynamic. The computational results show that the dynamic approach leads to higher water levels in the near-fault area. These significant differences only occur during the first instants of the surface deformation and level off later on. However it was also observed that the shape of the wave train can be altered by dynamical effects. Consequently the distinction between leading elevation wave and leading depression wave may not be as clear as anticipated. Of course the present method is computationally more expensive but there is an overall gain in accuracy. Not surprisingly more accurate tsunami computations require finer initial conditions such as those obtained by the active generation methodology used in the present study.

In future work we intend to extend this modeling to three space dimensions since it is evident that the 2D computations presented in this article have little interest beyond academics. Moreover we intend to use the exact results of Tadepalli & Synolakis [22,23] to check how different the runup may be for the two different initial waves (resulting from the passive and dynamic seafloor displacements) in an idealized basin similar to the one used by Okal & Synolakis [18].

14

Acknowledgments

References

[1] F. Benkhaldoun and L. Quivy, A non homogeneous Riemann solver for shallow water and two phase flows, Flow, Turbulence and Combustion 76 (2006) 391-402.

[2] Dutykh D. & Dias F., Water waves generated by a moving bottom, Tsunami and Nonlinear waves, Editor: Kundu Anjan, Springer Verlag (Geo Sc.) (2007) 63–94.

[3] Dutykh D., Dias F. & Kervella Y., Linear theory of wave generation by a moving bottom, C. R. Acad. Sci. Paris, Ser. I 343 (2006) 499–504.

[4] L. B. Freund, D. M. Barnett, A two-dimensional analysis of surface deformation due to dip-slip faulting, Bull. Seism. Soc. Am. 66 (1976) 667–675.

[5] J.-M. Ghidaglia, A. Kumbaro, G. Le Coq, On the numerical solution to two fluid models via cell centered finite volume method, Eur. J. Mech. B/Fluids 20 (2001) 841-867.

[6] J.-M. Ghidaglia, F. Pascal, The normal flux method at the boundary for multidimensional finite volume approximations in CFD, Eur. J. Mech. B/Fluids 24 (2005) 1–17.

[7] J. Hammack, A note on tsunamis: their generation and propagation in an ocean of uniform depth, J. Fluid Mech. 60 (1973) 769–799.

[8] N. A. Haskell, Elastic displacements in the near-field of a propagating fault, Bull. Seism. Soc. Am. 59 (1969) 865–908.

[9] F. Hecht, O. Pironneau, A. Le Hyaric, K. Ohtsuka, FreeFem++, Laboratoire JL Lions, University of Paris VI, France.

[10] K. Kajiura, Tsunami source, energy and the directivity of wave radiation, Bull. Earthquake Research Institute 48 (1970) 835–869.

[11] Kervella Y., Dutykh D. & Dias F., Comparison between three-dimensional linear and nonlinear tsunami generation models, Theor. Comput. Fluid Dyn. 21 (2007) 245–269.

[12] R. Madariaga, Radiation from a finite reverse fault in half space, Pure Appl. Geophys. 160 (2003) 555-577.

[13] L. Mansinha, D. E. Smylie, The displacement fields of inclined faults, Bull. Seism. Soc. Am. 61 (1971) 1433–1440.

[14] T. Masterlark, Finite element model predictions of static deformation from dislocation sources in a subduction zone: Sensivities to homogeneous, isotropic, Poisson-solid, and half-space assumptions, J. Geophys. Res. 108 (2003) 2540.

[15] A. Megna, S. Barba, S. Santini, Normal-fault stress and displacement through finite-element analysis, Annals Geophys. 48 (2005) 1009-1016.

[16] T. Ohmachi, H. Tsukiyama, H. Matsumoto, Simulation of tsunami induced by dynamic displacement of seabed due to seismic faulting, Bull. Seism. Soc. Am. 91 (2001) 1898–1909.

[17] Y. Okada, Surface deformation due to shear and tensile faults in a half-space, Bull. Seism. Soc. Am. 75 (1985) 1135–1154.

[18] E.A. Okal, C.E. Synolakis, Source discriminants for near-field tsunamis, Geophys. J. Int 158 (2004) 899–912.

[19] Y. Okumura, Y. Kawata, Effects of rise time and rupture velocity on tsunami, Proc. 17th Int. Offshore and Polar Engineering Conf., Vol. III (2007).

[20] J. Quiblier, Propagation des ondes en géophysique et en géotechnique. Modélisation par méthodes de Fourier, Paris: Editions Technip (1997).

[21] C.E. Synolakis, E.N. Bernard, Tsunami science before and beyond Boxing Day 2004, Phil. Trans. R. Soc. A 364 (2006) 2231–2265.

[22] S. Tadepalli, C.E. Synolakis, The runup of N-waves, Proc. R. Soc. London A 445 (1994) 99–112.

[23] S. Tadepalli, C.E. Synolakis, Model for the leading waves of tsunamis, Phys. Rev. Lett. 77 (1996) 2141–2144.

[24] M. I. Todorovska, M. D. Trifunac, Generation of tsunamis by a slowly spreading uplift of the sea floor, Soil Dynamics and Earthquake Engineering 21 (2001) 151–167.

[25] V.V. Titov, C.E. Synolakis, Numerical modeling of tidal wave runup, J. Waterway, Port, Coastal, and Ocean Engineering 124 (1998) 157–171.